

Contents lists available at ScienceDirect

# Journal of Computational Physics

www.elsevier.com/locate/jcp



# Construction of a peridynamic model for viscous flow



Jiangming Zhao<sup>a</sup>, Adam Larios<sup>b</sup>, Florin Bobaru<sup>a,\*</sup>

- <sup>a</sup> Department of Mechanical & Materials Engineering, University of Nebraska-Lincoln, Lincoln, NE, 68588-0526, USA
- <sup>b</sup> Department of Mathematics, University of Nebraska-Lincoln, Lincoln, NE 68588-0130, USA

### ARTICLE INFO

Article history:
Received 9 November 2021
Received in revised form 11 June 2022
Accepted 24 July 2022
Available online 29 July 2022

Keywords:
Peridynamics
Navier-Stokes equations
Nonlocal model
Viscous fluid
Incompressible flow
Poiseuille flow

#### ABSTRACT

We derive the Eulerian formulation for a peridynamic (PD) model of Newtonian viscous flow starting from fundamental principles: conservation of mass and momentum. This formulation is nonlocal, different from viscous flow models that utilize numerical methods like, e.g., the so-called "peridynamic differential operator" to approximate solutions of the classical Navier-Stokes equations. We show that the classical continuity equation is a limiting case of the PD one, assuming certain smoothness conditions. The PD model for viscous flow is calibrated by enforcing linear consistency for the viscous stress term with the classical Navier-Stokes equations. Couette and Poiseuille flows, and incompressible fluid flow past a regular lattice of cylinders are used to verify the new formulation, at low Reynolds numbers. The constructive approach in deriving the model allows for a seamless coupling with peridynamic models for corrosion or fracture for simulating complex fluid-structure interaction problems in which solid degradation takes place, such as in erosion-corrosion, hydraulic fracture, etc. Moreover, the new formulation sheds light on the relationships between local and nonlocal models.

© 2022 Elsevier Inc. All rights reserved.

# 1. Introduction

Nonlocality plays important roles in many phenomena, including anomalous diffusion [1,2] and turbulence in fluid motion [3–5], and effects of microstructure in the deformation and fracture of solid materials [6,7]. Classical models based on PDEs have difficulties dealing with problems involving nonlocal effects. Fractional calculus is a powerful mathematical tool that can describe nonlocal behavior. However, models based on fractional calculus are computationally costly because the integrals in fractional calculus are defined over the entire space [8]. The peridynamic (PD) theory, which was introduced as a nonlocal extension of the classical continuum mechanics [9], provides an alternative to fractional calculus. It has been shown that PD operators converge to corresponding classical and fractional operators as the nonlocal size  $\delta$  approaches zero and infinity, respectively [8,10]. Therefore, both classical and fractional operators can be seen as limiting cases of PD operators.

In addition to describing anomalous phenomena, PD models can be advantageous in simulating regular/common but complex physical/chemical problems. For example, classical local models have difficulties dealing with problems involving discontinuities or moving boundaries, such as those occurring in fracture, corrosion, etc. PD models, however, do not have such issues because they employ integro-differential equations (IDEs) rather than partial differential equations (PDEs), and thus cracks and other forms of damage can initiate and propagate naturally and autonomously [9,11,12]. Classical formula-

E-mail address: fbobaru2@unl.edu (F. Bobaru).

<sup>\*</sup> Corresponding author.

tions also encounter significant challenges for problems that involve complex interactions between fluids and solids, such as erosion corrosion and hydraulic fracture, while PD models, due to their generality/flexibility, have the potential to better deal with such problems [13,14].

While the PD method has been used extensively for mechanical and diffusion-type problems involving cracks and damage [15,16], there is very little existing literature on formulations or applications of the PD method to fluid mechanics, Statebased PD models for fluid flow in porous media are presented in [13,14,17] and are coupled with mechanical models to simulate the fluid-driven cracks [13,14]. These models are limited to porous flows in which the flow is driven by the pressure gradient. Later, more general models for fluid flow based on the Navier-Stokes equations (NSEs) have been developed in the PD framework to simulate laminar fluid flows at low Reynold numbers. Some of them make use of the PD correspondence model [18], such as the updated Lagrangian particle hydrodynamics (ULPH) [19-22] and the PD Moving Particle Semiimplicit (MPS) model [23].

An important distinction needs to be drawn between ordinary PD state-based models, and correspondence models. The latter generally result in non-ordinary state-based PD models. They employ a "translation" between PD forces/displacements and the classical tensor-representation of stresses and strains, the main goal being to reuse existing classical constitutive models. Stresses and strains, being second-order tensors, are linear mappings (therefore continuous), in contrast with PD forces/displacement fields which are more general constructs, nonlinear mappings, allowing for representing very general material behavior, including discontinuities. According to [24,25], the discretized PD correspondence models are equivalent to SPH and RKPM under certain conditions, and thus share some common numerical issues such as zero-energy modes.

We also note the use of the "PD differential operators" [26,27] and the "peridynamic D operators" [28] to compute derivatives using integral operators. It is important to clarify that these are "nonlocal numerical methods" that are used to solve local models (based on PDEs), quite different from a nonlocal model (like PD, which does not employ spatial derivatives).

The goal of our manuscript is to formulate (from basic principles) a new nonlocal (or peridynamic) version of the local NSEs and introduce numerical algorithms to compute approximate solutions to these new equations. The nonlocal NSEs can be useful in a variety of important applications, including fluid-structure interactions which lead to damage in the structure (e.g., hydraulic fracture and erosion-corrosion), modeling of complex fluids flow [29], etc.

It is worth noting that a PD formulation of the Navier-Stokes equations is perhaps a more natural model for fluids. First, we note that it is more general (at least formally), in the sense that it contains the classical Navier-Stokes equations as a special case (again, at least formally) by making a special choice of the PD kernel. Second, while proving (or disproving) the existence and uniqueness of global strong solutions to the classical incompressible 3D Navier-Stokes equations remains a challenging open problem, there is at least some hope that for a nonlocal PD formulation, such as the one presented in the present work, will allow for a proof of existence and uniqueness, at least for certain kernels. For instance, by analogy, it has been proven in [30] that a certain non-local version of the inviscid Burgers equation is globally well-posed, even though the classical version develops a singularity in finite time (see also [31] and the references therein). Third, on a deeper level, it may be that certain fluid regimes are more accurately described by taking into account non-local interactions rather than insisting that a strict local balance be maintained at every point in space and time, which in turn necessitates that solutions have at least some degree of smoothness (possibly in a weak sense) in order to make sense of the equations. For instance, it was noted by Ciprian Foias [32] that since (i) one can prove global well-posedness for the (modified) Navier-Stokes equations with higher-order diffusion added, (ii) higher-order diffusion modifications have been used with some success in certain ocean models, and (iii) higher-order derivatives have larger stencils (one pictures larger horizon sizes), there is some indication that including non-local interactions (in addition to the nonlocal effects of the pressure) could perhaps provide a model that more realistically captures the true dynamics of the flow.

In this work, we construct, for the first time, a PD bond-based model using the Eulerian description for viscous flow, starting from fundamental conservation principles, in order to arrive at a PD counterpart of the classical Navier-Stokes equation. We investigate the convergence of the terms in the PD continuity equation to their classical counterparts as the nonlocal size in PD equations approaches zero. (In forthcoming works, e.g., [33], we will study the convergence of solutions of the PD equations to solutions of the classical equations.). We test the PD model numerically using examples for which (classical) analytical or numerical solutions are available in the literature.

This paper is organized as follows: in Section 2 we introduce the constructive approach to arrive at the PD formulation for viscous flow and show convergence to the classical Navier-Stokes equations in the limit of the horizon going to zero; in Section 3 we explain the numerical discretization used; in Section 4 we verify our model for several problems with classical analytical/SPH solutions; conclusions are given in Section 5.

## 2. Peridynamic constructive model for viscous flow

In the classical theory of fluid mechanics, the motion of Newtonian fluids, in its Eulerian form, is described by the following NSEs [46]:

$$\frac{\partial \rho}{\partial t} = -\nabla \cdot (\rho \mathbf{v}) \tag{1}$$

$$\frac{\partial \rho}{\partial t} = -\nabla \cdot (\rho \mathbf{v}) 
\frac{\partial (\rho \mathbf{v})}{\partial t} = -\nabla \cdot (\rho \mathbf{v} \otimes \mathbf{v}) - \nabla p + \mu \nabla^2 \mathbf{v} + \rho \mathbf{b}$$
(1)

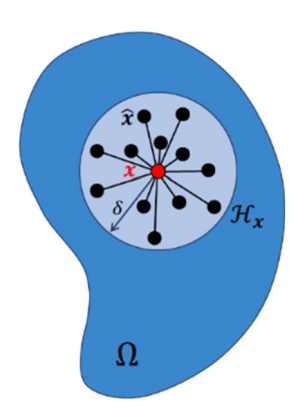


**Fig. 1.** A peridynamic body with a generic point x and its horizon  $\mathcal{H}_x$ . Nonlocal interactions exist through the bond between two points, e.g., point x and an arbitrary point  $\hat{x}$  located in its horizon  $\mathcal{H}_x$ .

where  $\rho$  is the density,  $\mathbf{v}$  is the velocity, p is the pressure,  $\mu$  is the viscosity and  $\mathbf{b}$  is a given body force density. These equations are derived from conservation principles of mass and momentum [46]. Note that an appropriate constitutive law is required to solve the above NSEs (e.g., constant  $\rho$  for incompressible fluids or equation of state for compressible fluids).

In this section, we derive an Eulerian PD model for viscous flow from a general PD continuity equation, following a procedure similar to that used in the derivation of the classical Eulerian Navier-Stokes equations.

Consider d=2 or 3, and let  $\Omega$  denote an open bounded subset of  $\mathbb{R}^d$ . Points in  $\mathbb{R}^d$  are denoted by the vectors  $\mathbf{x}$  or  $\hat{\mathbf{x}}$ . Functions from  $\Omega$ , or subsets of  $\Omega$ , and time  $t \in [0,T]$  into  $\mathbb{R}$  or  $\mathbb{R}^d$  are denoted by Roman or Greek letters, plain-face italic for scalars and lower-case bold italic for vectors, e.g.,  $\theta(\mathbf{x},t)$  and  $\mathbf{v}(\mathbf{x},t)$ . For notation simplicity, in much of the rest of the paper, we omit the spatial and temporal dependencies of these functions. For example, we denote  $\theta$  and  $\hat{\theta}$  for  $\theta(\mathbf{x},t)$  and  $\theta(\hat{\mathbf{x}},t)$ , respectively.

In PD models, each material point  $\mathbf{x} \in \Omega$  interacts with other points within its neighborhood  $\mathcal{H}_{\mathbf{x}}$ , which is called the horizon region of  $\mathbf{x}$  and is usually selected to be a disk when d=2 (or sphere when d=3) centered at  $\mathbf{x}$ . For a modification of this formulation to allow use of non-spherical horizons, please see [45] The radius of  $\mathcal{H}_{\mathbf{x}}$  is called the horizon size (or simply "the horizon") and denoted by  $\delta$ . Objects that carry the pairwise nonlocal interactions between points are called PD bonds. Fig. 1 schematically shows a peridynamic body with a generic point  $\mathbf{x}$ , its family and its horizon.

## 2.1. The peridynamic continuity equation

Bonds in PD models for solids are representations of force interactions between material points, in a sense similar to how atomic bonds act between atoms, molecular bonds between molecules, etc. PD models assume long-range interactions even at larger scales, and this is extremely useful when modeling damage initiation and its evolution using, for example, the meshfree discretization of the PD equations, because it removes geometrical constraints present in other numerical methods, like the Finite Element Method. For fluids, such long-range interactions can be useful when modeling, for example, fluid-structure interaction that leads to damage in the structure, corrosion/erosion under flow, complex fluids (fluids with particles), etc. For solids, nonlocality helps in homogenizing microstructures [6,34,35] and predict the complex evolution of damage and cracks in a variety of materials [7,36–38]. While a Lagrangian formulation for PD models of solids is natural, for fluids an Eulerian representation is more appropriate and will be used in this work. Eulerian-type PD models have been used before in heat and mass transfer as well as corrosion damage models, based on the concept of "diffusion PD bonds", which can be thought of as "pipes" through which "fluxes" are flowing, allowing points in the domain to interact with one another [39–42]. When we derive the PD formulation of mass conservation in this work, we use a similar concept for mass transport. For corrosion problems, the mass transfer model was complemented by damage and phase-change models [43–45].

To construct a bond-based PD model for fluid motion, we first consider an imaginary cylinder in a fluid domain with two points  $\mathbf{x}$  and  $\hat{\mathbf{x}}$  located at the top and bottom of the cylinder, respectively, as shown in Fig. 2. It is assumed that no mass transfer takes place through the cylinder's side surface. Even if the flow velocity has a component perpendicular to the axial direction of the cylinder, it does not participate in the transport of mass through the cylinder. Then, the continuity equation for some integrated property  $\theta$  (mass, linear momentum, etc.) associated with the fluid, in the Eulerian form, can be expressed by:

$$hs\frac{\partial \theta_a}{\partial t} + s\left(\hat{\theta}\,\hat{\mathbf{v}} - \theta\,\mathbf{v}\right) \cdot \mathbf{e} = hsr_a \tag{3}$$

where h and s are the height and cross-sectional area of the cylinder, respectively;  $\theta_a$  and  $r_a$  are the average  $\theta$  and source/sink (taking the source as positive) in the cylinder, respectively;  $\mathbf{v}$  is the flow velocity of the fluid;  $\mathbf{e}$  is the unit vector  $\frac{\hat{\mathbf{x}} - \mathbf{x}}{\|\hat{\mathbf{x}} - \mathbf{x}\|}$ . Since  $h = \|\hat{\mathbf{x}} - \mathbf{x}\|$ , dividing Eq. (3) by both h and s gives us:

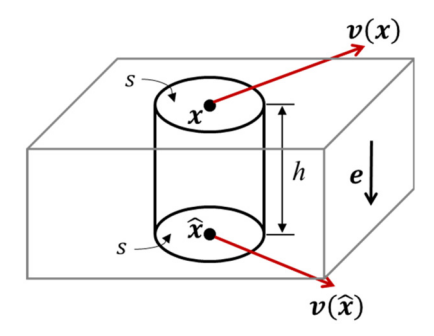


**Fig. 2.** A cylinder in the fluid domain with two points  $\mathbf{x}$  and  $\hat{\mathbf{x}}$  located at the top and bottom. It is assumed that nothing can transfer through the cylinder's side surface.

$$\frac{\partial \theta_a}{\partial t} + \frac{\hat{\theta} \hat{\mathbf{v}} - \theta \mathbf{v}}{\|\hat{\mathbf{x}} - \mathbf{x}\|} \cdot \mathbf{e} = r_a. \tag{4}$$

By taking  $\hat{x}$  to x, we would recover the classical derivation of the conservation equation. Instead, we assume the equation to hold for finite distances  $\|\hat{x} - x\|$ .

In the peridynamic framework, each material point  $x \in \Omega$  interacts with points located in  $\mathcal{H}_x$  through PD bonds. For each of these PD bonds, we assume that there is only mass transfer between PD points, which allows us to use Eq. (4). For the bond connecting  $\hat{x}$  and x, we can then write:

$$\frac{\partial \theta_a}{\partial t} + \alpha \frac{\hat{\theta} \, \hat{\mathbf{v}} - \theta \, \mathbf{v}}{\|\hat{\mathbf{x}} - \mathbf{x}\|} \cdot \mathbf{e} = r_a \tag{5}$$

where  $\alpha$  is a coefficient which connects the macroscale flow velocity to the bond-level flow velocity. It will be determined later by requiring that the PD equation/solution converges (see Section 2.2) to the classical one as  $\delta$  goes to zero. Note that  $\alpha$  can be selected as a function of  $\|\hat{\mathbf{x}} - \mathbf{x}\|$  as well [39], but this is not considered in this work for simplicity. Integrating Eq. (5) over the horizon of point  $\mathbf{x}$  we get:

$$\int_{\mathcal{H}_{\mathbf{x}}} \frac{\partial \theta_{a}}{\partial t} d\hat{\mathbf{x}} + \alpha \int_{\mathcal{H}_{\mathbf{x}}} \frac{\hat{\theta} \hat{\mathbf{v}} - \theta \mathbf{v}}{\|\hat{\mathbf{x}} - \mathbf{x}\|} \cdot \mathbf{e} d\hat{\mathbf{x}} = \int_{\mathcal{H}_{\mathbf{x}}} r_{a} d\hat{\mathbf{x}}$$
(6)

We assume the following relation between  $\theta$  at point x and time t and the average  $\theta$  in all the PD bonds connected at x:

$$\int_{\mathcal{H}_{\mathbf{x}}} \theta_{\mathbf{a}} d\hat{\mathbf{x}} = \theta \, \mathbf{V}_{\mathcal{H}} \tag{7}$$

where  $V_{\mathcal{H}}$  is the volume (area in 2D and length in 1D) of the horizon region, a constant in this paper. Then we can write:

$$\int_{\mathcal{H}_{\mathbf{x}}} \frac{\partial \theta_a}{\partial t} d\hat{\mathbf{x}} = \frac{\partial \theta}{\partial t} V_{\mathcal{H}}$$
(8)

Similarly, we have:

$$\int_{\mathcal{H}_{\sigma}} r_{\mathbf{d}} \hat{\mathbf{x}} = r V_{\mathcal{H}} \tag{9}$$

Therefore, Eq. (6) becomes:

$$\frac{\partial \theta\left(\mathbf{x},t\right)}{\partial t} = -\frac{\alpha}{V_{\mathcal{H}}} \int_{\mathcal{H}_{c}} \frac{\theta\left(\hat{\mathbf{x}},t\right) \mathbf{v}\left(\hat{\mathbf{x}},t\right) - \theta\left(\mathbf{x},t\right) \mathbf{v}\left(\mathbf{x},t\right)}{\|\hat{\mathbf{x}}-\mathbf{x}\|} \cdot \mathbf{e}\left(\mathbf{x},\hat{\mathbf{x}}\right) d\hat{\mathbf{x}} + r\left(\mathbf{x},t\right)$$
(10)

which is the general PD continuity equation in Eulerian form.

In the next section, we first show that the classical continuity equation is a limiting case of the PD form in Eq. (6). This is achieved by showing that the PD continuity equation converges to that of the classical one as  $\delta \to 0$ .

# 2.2. Convergence of the peridynamic continuity equation to the classical one

To simplify the writing, we use the following notation for the weight function:

$$\omega = \omega \left( \mathbf{x}, \hat{\mathbf{x}} \right) = \frac{\alpha}{V_{\mathcal{H}} \left\| \hat{\mathbf{x}} - \mathbf{x} \right\|}$$
(11)

and for the nonlocal gradient and divergence operators:

$$\mathcal{G}_{\omega}\left(\phi\right)\left(\mathbf{x}\right) = \int_{\mathcal{H}_{\mathbf{x}}} \omega\left(\phi\left(\hat{\mathbf{x}},t\right) - \phi\left(\mathbf{x},t\right)\right) \mathbf{e} d\hat{\mathbf{x}} \tag{12}$$

$$\mathcal{D}_{\omega}\left(\boldsymbol{\varphi}\right)\left(\boldsymbol{x}\right) = \int_{\mathcal{H}_{\boldsymbol{x}}} \omega\left(\boldsymbol{\varphi}\left(\hat{\boldsymbol{x}},t\right) - \boldsymbol{\varphi}\left(\boldsymbol{x},t\right)\right) \cdot \boldsymbol{e} d\hat{\boldsymbol{x}}$$
(13)

where  $\phi$  and  $\varphi$  are some arbitrary scalar and vector fields in  $L^2$ , respectively. The weighted nonlocal operators  $\mathcal{G}_{\omega}(\phi)$  and  $\mathcal{D}_{\omega}(\varphi)$  have been shown (see Section 5.2 in [47]) to converge (in the  $L^2$  norm) to their differential counterparts  $\nabla \phi$  and  $\nabla \cdot \varphi$ , respectively, as  $\delta \to 0$  ( $\delta$ -convergence), if the weight function satisfies the following condition:

$$\int_{\mathcal{H}_{\mathbf{x}}} \omega \|\hat{\mathbf{x}} - \mathbf{x}\| \, \mathrm{d}\hat{\mathbf{x}} = d \tag{14}$$

in which d is the dimension. Substitute Eq. (11) into Eq. (14) leads to  $\alpha = d$ . In Appendix A, as an illustration, we use simple Taylor expansions to show that  $\mathcal{G}_{\omega}(\phi)$  converges to  $\nabla \phi$  when  $\alpha = d$ . For more detailed proofs of convergence in the  $L^2$  norm for both nonlocal gradient and divergence, the reader is referred to [47].

Using the nonlocal operators defined in Eqs. (12) and (13), the integral in Eq. (10) can be written as:

$$\mathcal{D}_{\omega}(\theta \mathbf{v}) = \int_{\mathcal{H}_{\mathbf{x}}} \omega \left( \hat{\theta} \, \hat{\mathbf{v}} - \theta \mathbf{v} \right) \cdot \mathbf{e} d\hat{\mathbf{x}}$$

$$= \int_{\mathcal{H}_{\mathbf{x}}} \omega \left( \hat{\theta} \, \left( \hat{\mathbf{v}} - \mathbf{v} \right) - \theta \, \left( \hat{\mathbf{v}} - \mathbf{v} \right) + \theta \, \left( \hat{\mathbf{v}} - \mathbf{v} \right) + \mathbf{v} \, \left( \hat{\theta} - \theta \right) \right) \cdot \mathbf{e} d\hat{\mathbf{x}}$$

$$= \mathbf{v} \cdot \mathcal{G}_{\omega}(\theta) + \theta \mathcal{D}_{\omega}(\mathbf{v}) + \mathcal{A}_{\omega}(\theta, \mathbf{v})$$
(15)

in which the last term is

$$\mathcal{A}_{\omega}(\theta, \mathbf{v}) = \int_{\mathcal{U}} \omega \left(\hat{\theta} - \theta\right) \left(\hat{\mathbf{v}} - \mathbf{v}\right) \cdot \mathbf{e} d\hat{\mathbf{x}}$$
(16)

Therefore, Eq. (10) can be written as:

$$\frac{\partial \theta \left( \mathbf{x}, t \right)}{\partial t} = -\mathbf{v} \cdot \mathcal{G}_{\omega} \left( \theta \right) - \theta \mathcal{D}_{\omega} \left( \mathbf{v} \right) + \mathcal{A}_{\omega} \left( \theta, \mathbf{v} \right) + r \left( \mathbf{x}, t \right) \tag{17}$$

We show that  $\mathcal{A}_{\omega}(\theta, \mathbf{v}) \to 0$  as  $\delta \to 0$ , as follows:

$$\mathcal{A}_{\omega}(\theta, \mathbf{v}) = \int_{\mathcal{H}_{\mathbf{x}}} \omega \left(\hat{\theta} - \theta\right) (\hat{\mathbf{v}} - \mathbf{v}) \cdot \mathbf{e} d\hat{\mathbf{x}}$$

$$\leq \int_{\mathcal{H}_{\mathbf{x}}} \left| \omega \left(\hat{\theta} - \theta\right) (\hat{\mathbf{v}} - \mathbf{v}) \cdot \mathbf{e} \right| d\hat{\mathbf{x}}$$

$$\leq \int_{\mathcal{H}_{\mathbf{x}}} \left| \omega \right| \left| \left(\hat{\theta} - \theta\right) \right| \|\hat{\mathbf{v}} - \mathbf{v}\| d\hat{\mathbf{x}}$$

$$\leq \frac{d}{V_{\mathcal{H}}} \int_{\mathcal{H}_{\mathbf{x}}} \frac{1}{\|\hat{\mathbf{x}} - \mathbf{x}\|} \left| \left(\hat{\theta} - \theta\right) \right| \|\hat{\mathbf{v}} - \mathbf{v}\| d\hat{\mathbf{x}}$$

$$(18)$$

According to Taylor's theorem and the Cauchy-Schwarz inequality, we have on  $\mathcal{H}_x$ :

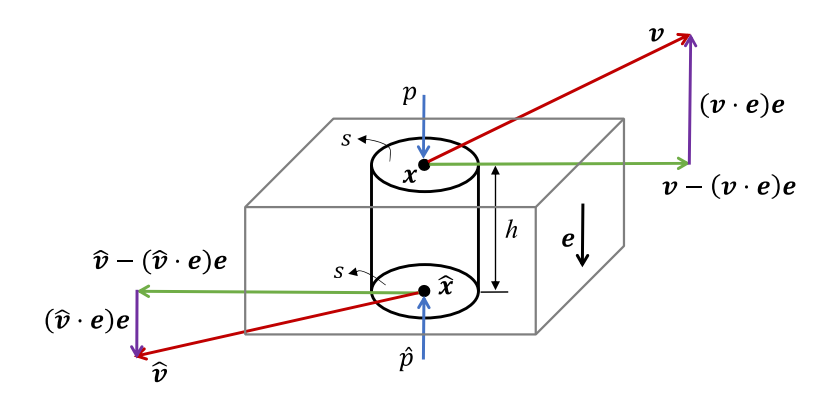


Fig. 3. Velocity decomposition at x and  $\hat{x}$  located at the top and bottom, respectively, for an imaginary cylinder in the fluid domain.

$$\frac{\left|\hat{\theta} - \theta\right|}{\left\|\hat{\boldsymbol{x}} - \boldsymbol{x}\right\|} \le \left\|\nabla\theta\right\| + \frac{1}{2} \left\|\nabla^2\theta\right\| \left\|\hat{\boldsymbol{x}} - \boldsymbol{x}\right\| + O\left(\left\|\hat{\boldsymbol{x}} - \boldsymbol{x}\right\|\right) \le \left\|\nabla\theta\right\| + \frac{\delta}{2} \left\|\nabla^2\theta\right\| + O\left(\delta\right)$$

$$\tag{19}$$

and

$$\|\hat{\mathbf{v}} - \mathbf{v}\| \le \|D\mathbf{v}\| \|\hat{\mathbf{x}} - \mathbf{x}\| + O(\|\hat{\mathbf{x}} - \mathbf{x}\|) \le \|D\mathbf{v}\| \delta + O(\delta)$$
 (20)

where

$$D\mathbf{v} = \frac{\partial v^i}{\partial x^j} \mathbf{e}_i \otimes \mathbf{e}^j \tag{21}$$

If  $D\mathbf{v}$  and  $\nabla \theta$  are bounded in  $\Omega$ , we have:

$$\mathcal{A}_{\omega}(\theta, \mathbf{v}) \le d\left(\|\nabla\theta(\mathbf{x})\| + \frac{\delta}{2} \|\nabla^{2}\theta(\mathbf{x})\| + O(\delta)\right) (\|D\mathbf{v}(\mathbf{x})\| \delta + O(\delta)) \to 0 \quad \text{as } \delta \to 0$$
(22)

Comparing the PD form of continuity equation in Eq. (17) with its classical form:

$$\frac{\partial \theta}{\partial t} = -\mathbf{v} \cdot \nabla \theta - \theta \nabla \cdot \mathbf{v} + r,\tag{23}$$

and considering that  $\mathcal{G}_{\omega}\left(\theta\right)\to\nabla\theta$  and  $\mathcal{D}_{\omega}\left(\mathbf{v}\right)\to\nabla\cdot\mathbf{v}$  in the sense of  $L^{2}$  as  $\delta\to0$ , we conclude that the PD continuity equation converges to the classical version as  $\delta\to0$ .

### 2.3. The peridynamic formulation for viscous flow

Starting from the general continuity equation given in Eq. (10), we now derive the PD governing equations for viscous flow. When the property  $\theta$  in Eq. (10) is mass, by taking r = 0, we obtain the PD mass continuity equation without sources/sinks:

$$\frac{\partial \rho}{\partial t} = -\frac{d}{V_{\mathcal{H}}} \int_{\mathcal{H}_{\mathbf{x}}} \frac{\hat{\rho} \hat{\mathbf{v}} - \rho \mathbf{v}}{\|\hat{\mathbf{x}} - \mathbf{x}\|} \cdot \mathbf{e} d\hat{\mathbf{x}}$$
(24)

where  $\rho$  is the mass density. When the property  $\theta$  is the linear momentum, we have the following PD equation of motion:

$$\frac{\partial (\rho \mathbf{v})}{\partial t} = -\frac{d}{V_{\mathcal{H}}} \int_{\mathcal{H}} \frac{\hat{\rho} \hat{\mathbf{v}} \otimes \hat{\mathbf{v}} - \rho \mathbf{v} \otimes \mathbf{v}}{\|\hat{\mathbf{x}} - \mathbf{x}\|} \cdot \mathbf{e} d\hat{\mathbf{x}} + \mathbf{r}$$
(25)

in which the generic momentum source r consists of internal and external forces. The internal forces can be decomposed into pressure and viscous forces. To find the expression for these forces in the PD framework, we consider again the cylinder shown in Fig. 2. As shown in Fig. 3, in a viscous flow, the force exerted on the cylinder along its axial direction is:

$$s\left(\hat{p}-p\right)\boldsymbol{e}\tag{26}$$

The viscous force, inspired by the shear bond force introduced in PD bond-based mechanical models [48,49], can be formulated as the shear force exerted on the cylinder due to the velocity difference between the two ends of the cylinder:

$$\mu s \frac{(\mathbf{I} - \mathbf{e} \otimes \mathbf{e}) (\hat{\mathbf{v}} - \mathbf{v})}{\|\hat{\mathbf{x}} - \mathbf{x}\|} \tag{27}$$

in which  $\mu$  is the viscosity of the fluid, and  $(\mathbf{I} - \mathbf{e} \otimes \mathbf{e}) (\hat{\mathbf{v}} - \mathbf{v})$  is the portion of velocity difference, between the two ends of the cylinder, that is perpendicular to the cylinder's axial direction  $\mathbf{e}$ .

Following a similar procedure used to derive the general PD continuity equation as shown in Section 2.1, we have:

$$\mathbf{r} = -\frac{\alpha_{p}}{V_{\mathcal{H}}} \int_{\mathcal{H}_{\mathbf{x}}} \frac{\hat{p} - p}{\|\hat{\mathbf{x}} - \mathbf{x}\|} \cdot \mathbf{e} d\hat{\mathbf{x}} + \frac{\mu \alpha_{\mu}}{V_{\mathcal{H}}} \int_{\mathcal{H}_{\mathbf{x}}} \frac{\left( (\mathbf{I} - \mathbf{e} \otimes \mathbf{e}) \left( \hat{\mathbf{v}} - \mathbf{v} \right) \right)}{\|\hat{\mathbf{x}} - \mathbf{x}\|^{2}} d\hat{\mathbf{x}} + \rho \mathbf{b}$$
(28)

Therefore, the PD governing equations for viscous flow are established as follows:

$$\frac{\partial \rho \left(\mathbf{x}, t\right)}{\partial t} = -\frac{d}{V_{\mathcal{H}}} \int_{\mathcal{H}_{\mathbf{x}}} \frac{\hat{\rho} \hat{\mathbf{v}} - \rho \left(\mathbf{x}, t\right) \mathbf{v} \left(\mathbf{x}, t\right)}{\|\hat{\mathbf{x}} - \mathbf{x}\|} \cdot \mathbf{e} \left(\mathbf{x}, \hat{\mathbf{x}}\right) d\hat{\mathbf{x}} 
= -\frac{d}{V_{\mathcal{H}}} \int_{\mathcal{H}_{\mathbf{x}}} \frac{\rho \left(\hat{\mathbf{x}}, t\right) \mathbf{v} \left(\hat{\mathbf{x}}, t\right) \otimes \mathbf{v} \left(\hat{\mathbf{x}}, t\right) - \rho \left(\mathbf{x}, t\right) \mathbf{v} \left(\mathbf{x}, t\right) \otimes \mathbf{v} \left(\mathbf{x}, t\right)}{\|\hat{\mathbf{x}} - \mathbf{x}\|} \cdot \mathbf{e} \left(\mathbf{x}, \hat{\mathbf{x}}\right) d\hat{\mathbf{x}} 
- \frac{\alpha_{p}}{V_{\mathcal{H}}} \int_{\mathcal{H}_{\mathbf{x}}} \frac{p \left(\hat{\mathbf{x}}, t\right) - p \left(\mathbf{x}, t\right)}{\|\hat{\mathbf{x}} - \mathbf{x}\|} \cdot \mathbf{e} \left(\mathbf{x}, \hat{\mathbf{x}}\right) d\hat{\mathbf{x}} 
+ \frac{\mu \alpha_{\mu}}{V_{\mathcal{H}}} \int_{\mathcal{H}_{\mathbf{x}}} \frac{\left(\left(\mathbf{I} - \mathbf{e} \left(\mathbf{x}, \hat{\mathbf{x}}\right) \otimes \mathbf{e} \left(\mathbf{x}, \hat{\mathbf{x}}\right)\right) \left(\mathbf{v} \left(\hat{\mathbf{x}}, t\right) - \mathbf{v} \left(\mathbf{x}, t\right)\right)\right)}{\|\hat{\mathbf{x}} - \mathbf{x}\|^{2}} d\hat{\mathbf{x}} 
+ \rho \left(\mathbf{x}, t\right) \mathbf{b} \left(\mathbf{x}, t\right) \tag{30}$$

The PD model for viscous flow contains the pressure field which does not have an explicit equation yet. For incompressible Newtonian fluids, because directly solving the original incompressible equations creates numerical difficulties in terms of accuracy and efficiency, the artificial compressibility method is commonly used in the literature to handle the pressure term (see, e.g., [50–52]). This approach treats the incompressible fluid as a weakly compressible one and adopts an equation of state to explicitly determine the pressure field from the density field [51,53] as follows:

$$p = \frac{\rho_0 c_0^2}{\gamma} \left( \left( \frac{\rho^*}{\rho_0} \right)^{\gamma} - 1 \right) \tag{31}$$

where  $\rho_0$  is the initial density,  $\rho^*$  is the predicted density at the current step,  $\gamma$  is the material constant which is 7 for water and  $c_0$  is the sound speed in the initial density. The real sound speed is usually not used as it would require a significantly small timestep for stability of the numerical model (see Section 3). Instead, an artificial, lower sound speed c, which ensures sufficiently accurate solution, is preferred. To keep the density variation of fluid to less than 1% of the initial density, the Mach number (M = v/c) must be smaller than 0.1 [51]. This requires the artificial sound speed to be higher than 10 times of the maximum fluid velocity.

The PD equations for viscous flow still require determination of the unknown parameters in the weight functions. We already know that  $\alpha=d$  from Section 2.2. Since  $\alpha_p$  in Eq. (30) is also a constant coefficient in the PD gradient operator, we have  $\alpha_p=\alpha=d$ . We find  $\alpha_\mu$  by calibration for a simple flow problem, that ensures linear consistency of the formulation [40,41]. Consider a steady-state shear-driven fluid flow parallel to the x-axis and with a linear distribution of velocity magnitude, i.e.,  $v=v_0y$ . According to Newton's law of viscosity, we have  $\tau_{xx}=\mu v_0$ . The counterpart of  $\tau_{xx}$  in PD can be formulated as  $\tau_{xx}^{PD}=\frac{\alpha_\mu\mu\nu_0}{10}$  for 3D and  $\tau_{xx}^{PD}=\frac{3}{16}\alpha_\mu\mu\nu_0$  for 2D. The detailed derivation of  $\tau_{xx}^{PD}$  is provided in Appendix A. By letting  $\tau_{xx}^{PD}=\tau_{xx}$ , we find  $\alpha_\mu=10$  for 3D and  $\alpha_\mu=\frac{16}{3}$  for 2D.

### 2.4. Boundary conditions

Unlike classical local methods, "boundary conditions" in peridynamics are "volume constraints", being applied through a finite layer under the surface of a body. However, in practice, measurements are normally achievable only at the surfaces of a body, thus the normal local representation of boundary conditions. For these reasons, imposing local-type boundary conditions in peridynamic models is usually desired/needed. Various methods to impose local boundary conditions in PD models have been investigated in [47,54,55]. One such method is the fictitious nodes method (FNM) [54–56]. In FNM for peridynamics, certain constraints are specified on the fictitious region  $\tilde{\Omega} = \{x \notin \Omega \mid \text{distance}\,(x, \partial\Omega) < \delta\}$  (the "collar"

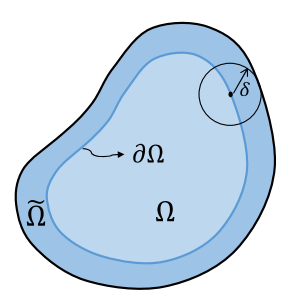


**Fig. 4.** Schematic of a peridynamic domain  $(\Omega)$ , its boundary  $(\partial\Omega)$ , and its fictitious region,  $\tilde{\Omega}$ .

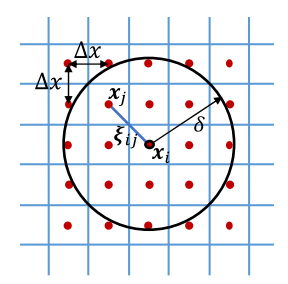


Fig. 5. Uniform discretization for the 2D PD model. The circular region is the horizon region of node  $x_i$ .

outside of the solution domain  $\Omega$  shown in Fig. 4), so that desired local boundary conditions imposed at  $\partial\Omega$  are satisfied or approximately satisfied. Fig. 4 schematically shows the solution domain  $\Omega$ , its boundary  $\partial\Omega$ , and the fictitious region,  $\tilde{\Omega}$ .

In fluid dynamics, there are a number of different boundaries conditions, such as inlet/outlet, free and solid wall boundaries [57]. Various treatments are required for each of these types. In this work, we only consider no-slip solid wall boundaries. The corresponding boundary conditions then are:

$$\mathbf{v} \cdot \mathbf{n} = 0$$

$$\mathbf{v} \cdot \mathbf{t} = 0$$
(32)

where n and t are vectors normal and tangential to the boundary, respectively. We use the naïve-type FNM (because of its ease of implementation, see [58]) to enforce the above boundary conditions, i.e., the velocity assigned to the fictitious points  $x \in \tilde{\Omega}$  are the same as that of the solid wall:

$$\mathbf{v}\left(\mathbf{x}\right) = \mathbf{v}_{\text{wall}} = \mathbf{0} \tag{33}$$

### 3. Numerical implementation

For the spatial discretization, we discretize the domain uniformly [59] into cells with nodes in the center of those cells. Fig. 5 shows a 2D uniform discretization with grid spacing  $\Delta x$  around a node  $x_i$ . Non-uniform grids are also possible [60–62], and very useful when having to conform to round boundaries [7,63], but this is not pursued in this work.

To discretize the peridynamic integro-differential equations, we use a meshfree method with one-point Gaussian quadrature [59] for the approximation of the integral term. For the time integration we select the forward-Euler method for simplicity.

The discretized PD equations for viscous flow (Eqs. (29) and (30)) are as follows:

$$\rho_{i}^{n+1} = \rho_{i}^{n} - \frac{d \Delta t}{\pi \delta^{2}} \sum_{\substack{j \in \mathcal{H}_{i} \\ j \neq i}} \left( \frac{\rho_{j}^{n} \mathbf{v}_{j}^{n} - \rho_{i}^{n} \mathbf{v}_{i}^{n}}{\xi_{ij}} \cdot \frac{\mathbf{x}_{j} - \mathbf{x}_{i}}{\xi_{ij}} V_{ij} \right)$$

$$\mathbf{v}_{i}^{n+1} = \mathbf{v}_{i}^{n} + \frac{\Delta t}{\rho_{i}^{n}} \left[ -\frac{d}{V_{\mathcal{H}}} \left( \sum_{\substack{j \in \mathcal{H}_{i} \\ j \neq i}} \frac{\left(\rho_{j}^{n} \mathbf{v}_{j}^{n} \otimes \mathbf{v}_{j}^{n} - \rho_{i}^{n} \mathbf{v}_{i}^{n} \otimes \mathbf{v}_{i}^{n}\right)}{\xi_{ij}} \cdot \xi_{ij} V_{ij} \right)$$

$$(34)$$

$$-\frac{d}{V_{\mathcal{H}}}\sum_{\substack{j\in\mathcal{H}_i\\j\neq i}}\left(\frac{\left(p_j^n-p_i^n\right)\boldsymbol{\xi}_{ij}}{\xi_{ij}^2}V_{ij}\right)$$

$$+\frac{\mu\alpha_{\mu}}{V_{\mathcal{H}}}\sum_{\substack{j\in\mathcal{H}_{i}\\j\neq i}}\frac{1}{\xi_{ij}^{2}}\left(\mathbf{I}-\frac{\boldsymbol{\xi}_{ij}\otimes\boldsymbol{\xi}_{ij}}{\xi_{ij}^{2}}\right)\cdot\left(\boldsymbol{v}_{j}^{n}-\boldsymbol{v}_{i}^{n}\right)V_{ij}+\rho_{i}^{n}\boldsymbol{b}_{i}^{n}$$
(35)

where  $\xi_{ij} = \mathbf{x}_j - \mathbf{x}_i$  and  $\xi_{ij} = ||\xi_{ij}||$ . The superscript n means  $n^{\text{th}}$  load step. The subscripts i and j denote the current node  $\mathbf{x}_i$  and its family node  $\mathbf{x}_j$  respectively, in the discretized domain.  $\mathcal{H}_i$  is the horizon region of node  $\mathbf{x}_i$ ,  $j \in \mathcal{H}_i$  includes all the nodes covered by  $\mathcal{H}_i$  (fully or partially),  $V_{ij}$  is the area of node  $\mathbf{x}_j$  covered by  $\mathcal{H}_i$ . Note that the partial volume integration, which was first proposed in [64] and then further discussed in [65,66], is used to approximate  $V_{ij}$ .

For stability of the time-integrator, the time step needs to satisfy several criteria. Here we use similar criteria as those in SPH models [52], including a CFL condition [67], the additional constraints due to the magnitude of nodal accelerations *a* [68] and the viscous diffusion, as follows:

$$\Delta t \le 0.25 \frac{\Delta x}{c} \tag{36}$$

$$\Delta t \le 0.25 \left(\frac{\Delta x}{a}\right)^{\frac{1}{2}} \tag{37}$$

$$\Delta t \le 0.125 \frac{\rho \Delta x^2}{\mu} \tag{38}$$

where the value of each right-hand side is the minimum over all nodes.

A detailed study of the stability, consistency, and convergence of the numerical scheme, and higher-order schemes, as well as simulations in the higher Reynolds number case, will be the subject of forthcoming work. Our purpose here is just to demonstrate that a straight-forward implementation agrees with some standard benchmark cases to a reasonable level of accuracy—a first step toward validation of the model.

### 4. Computational validation

In this section, we first verify our PD model for viscous flow using the Couette and Poiseuille flow problems. We test whether the PD solution converges, in the limit of horizon going to zero, to the classical analytical solutions. We also study the flow through a periodic array of cylinders to test the wall boundary condition for curved geometries and compare with an SPH solution (of the corresponding classical model) from the literature.

# 4.1. Couette flow

Consider two infinite, parallel plates separated by a distance h. The top one, moves with a constant velocity  $v_0$  in its own plane. This generates a unidirectional fluid motion, called Couette flow. The series solution for the classical model of this problem, in terms of the velocity in the horizontal direction, is given by [52]:

$$v_{x}(y,t) = \frac{v_{0}}{h}y + \sum_{n=1}^{\infty} \frac{2v_{0}}{n\pi} (-1)^{n} \sin\left(\frac{n\pi}{h}y\right) \exp\left(-\frac{\mu}{\rho} \frac{n^{2}\pi^{2}}{h^{2}}t\right)$$
(39)

In our PD simulation of this Couette flow problem, we choose  $v_0=10~\mu\text{m/s}$ , h=1~mm,  $\rho=10^3~\text{kg/m}^3$  and  $\mu=10^{-3}~\text{kg}\cdot\text{m}^{-1}\cdot\text{s}^{-1}$ . We make the domain periodic in the x direction to mimic the infinite domain (see Fig. 16 in [44] for an illustration of how this can be achieved). Fig. 6 shows the comparison of the velocity profile along y-axis between the PD solution (for  $\delta=40~\mu\text{m}$  and m=4) and the analytical series solution of the classical model at different times. A  $\delta$ -convergence study is then performed, and results are shown in Table 1. Note that the convergence rate of  $\delta$ -convergence is linear because we use the naïve FNM to impose the local boundary condition [58]. Higher convergence rate should be possible with the mirror-based FNM, for example, but this is not pursued here.

# 4.2. Poiseuille flow

The second test case is Poiseuille flow between stationary infinite plates at y = 0 and y = h. The fluid is initially at rest and is driven by an applied body force  $b_x$  parallel to the x-axis for  $t \ge 0$ . The series solution of the classical model for this problem give the velocity in the horizontal direction as [52]:

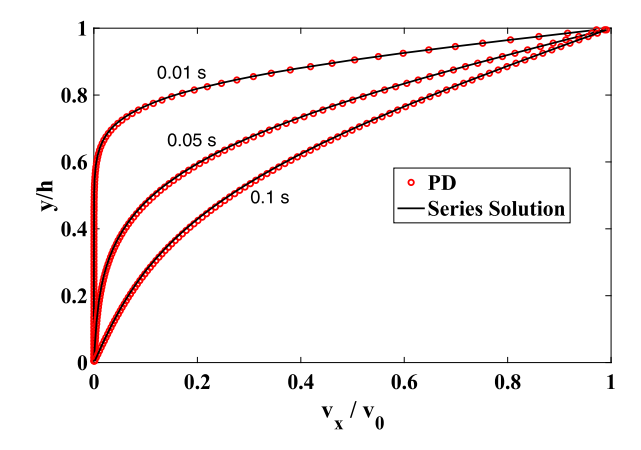
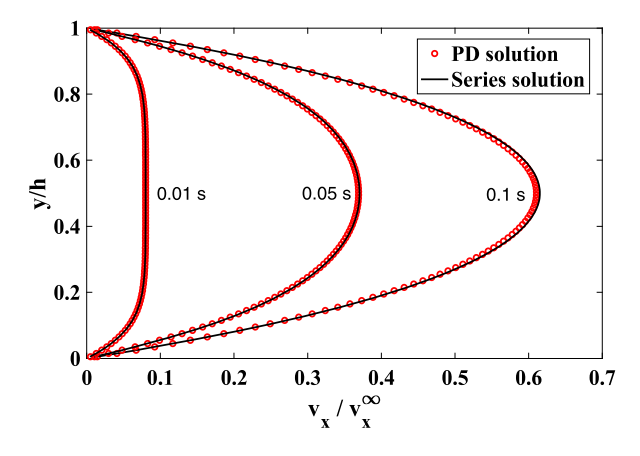


Fig. 6. Comparison of PD solutions (for  $\delta = 40~\mu m$  and m = 4) and series solutions of the corresponding classical model (using the first 50 terms in the series) for Couette flow.

**Table 1**  $\delta$ -convergence study for the PD solution of Couette flow.

t = 0.1  s	$\delta = 80 \ \mu m$	$\delta = 40 \ \mu m$	$\delta = 20 \ \mu m$
$\varepsilon_r$	0.0419	0.0184	0.0075

where  $\varepsilon_r = \frac{\sqrt{\sum_{i=1}^{n} (u_i^{\text{classical}} - u_i^{\text{PO}})^2}}{\sqrt{\sum_{i=1}^{n} (u_i^{\text{classical}})^2}}$ , and n is the total number of nodes used in the computation.



**Fig. 7.** Comparison of PD solutions (for  $\delta = 40~\mu m$  and m = 4) and series solutions of the corresponding classical model (using the first 50 terms in the series) for Poiseuille flow. Note that  $v_{\chi}^{\infty} = v_{\chi} \left(\frac{h}{2}, \infty\right) = \frac{\rho b_{\chi} h^2}{8\mu}$ .

$$v_{x}(y,t) = \frac{\rho b_{x}}{2\mu} y (h-y) + \sum_{n=0}^{\infty} \frac{4\rho b_{x} h^{2}}{\mu \pi^{3} (2n+1)^{3}} \sin\left(\frac{\pi y}{h} (2n+1)\right) \exp\left(-\frac{(2n+1)^{2} \pi^{2} \mu}{\rho h^{2}} t\right)$$
(40)

We choose h=1 mm,  $\rho=10^3$  kg/m<sup>3</sup>,  $\mu=10^{-3}$  kg·m<sup>-1</sup>·s<sup>-1</sup> and  $b_x=1\times10^{-4}$  m/s<sup>2</sup>. Again, the PD solution matches the series solution very well, as shown in Fig. 7.

# 4.3. Flow through a periodic lattice of cylinders

The previous examples have shown the performance of our method for fluid flow confined by straight channel walls. Now we verify the model for flow through a periodic array of disks/cylinders [52] (see Fig. 8), to test the wall boundary condition for curved geometries. For implementing periodic BCs in PD models, please see [44]. The parameters used in this example are given in Table 2. Fig. 9 shows the comparison for the velocity magnitude and velocity contour lines at steady state between PD results ( $100 \times 100$  discretization nodes) and SPH results ( $50 \times 50$  particles, plus extra particles placed on the circular disk to conform better to the actual geometry) from [69]. In spite of using a uniform discretization grid that does not conform with the circular disk geometry, the PD results track the SPH solution very well. As mentioned in

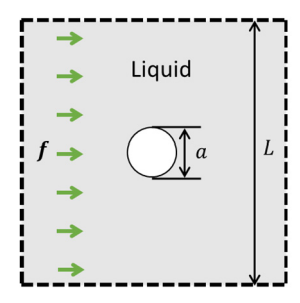
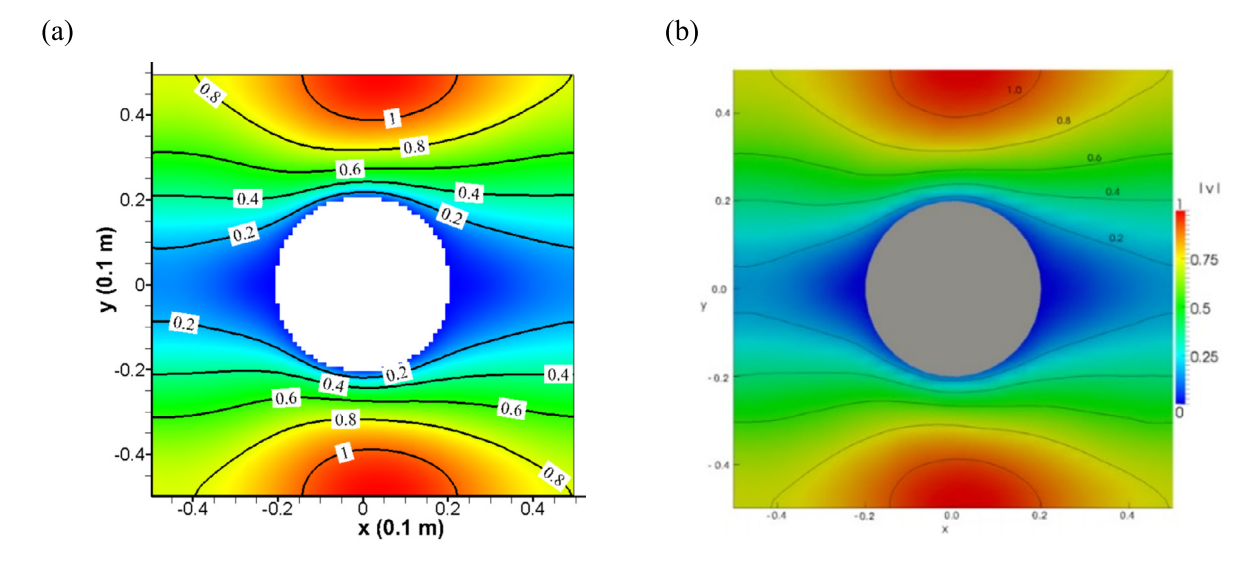


Fig. 8. Schematic of fluid flow driven by a body force around a disk. The cell is repeated by symmetry to represent flow around a periodic array of disks.

**Table 2** Parameters for flow through periodic lattice of disks.

Parameters	Value	Parameters	Value
L	0.1 m	а	$4 \times 10^{-2} \text{ m}$
$\mu$	$10^{-3} \text{ kg} \cdot \text{m}^{-1} \cdot \text{s}^{-1}$	f	$1.5 \times 10^{-7} \text{ m} \cdot \text{s}^{-2}$
ρ	$1 \text{ kg} \cdot \text{m}^{-3}$	с	$5.77 \times 10^{-4} \text{ m} \cdot \text{s}^{-1}$



**Fig. 9.** Contour plots of velocity magnitude by (a) PD model (for  $\delta = 40 \, \mu m$  and m = 4); (b) SPH model [69] (contour lines are labeled in units of  $10^{-4} \, \text{m/s}$ ). (For interpretation of the colors in the figure(s), the reader is referred to the web version of this article.)

Section 3, PD can also be implemented on non-uniform, conforming grids (see, e.g., [63]), but this is not pursued here for simplicity.

### 5. Conclusions

In this paper, we constructed a peridynamic (PD) alternative of the classical Navier-Stokes equations (in Eulerian formulation) from fundamental conservation principles. The formulation is different from "re-casting" of the classical Navier-Stokes equations using the so-called "PD differential operator" found in the literature. The classical continuity equation is shown to be a limiting case of the PD one with selected weight functions. The viscous force was formulated based on the PD shear bond forces. The weight function present in the viscous force was determined by enforcing linear consistency of the viscous stress provided by a PD model with that from a corresponding classical model. The model was verified against analytical solutions of the classical model for Couette and Poiseuille flows, as well as against an SPH approximation of the classical model for incompressible flow past a regular lattice of cylinders at low Reynolds numbers. The new model can be used to solve fluid-structure interaction problems involving damage and degradation, such as erosion, erosion-corrosion and hydraulic fracture, by coupling with existing PD models for corrosion and fracture.

### **CRediT** authorship contribution statement

**Jiangming Zhao:** Methodology, Software, Validation, Writing – original draft, Writing – review & editing. **Adam Larios:** Funding acquisition, Methodology, Writing – review & editing. **Florin Bobaru:** Conceptualization, Funding acquisition, Methodology, Project administration, Supervision, Writing – review & editing.

### **Declaration of competing interest**

The authors declare that they have no known competing financial interests or personal relationships that could have appeared to influence the work reported in this paper.

# Acknowledgements

This work has been supported in part by the US National Science Foundation Grant No. 1953346. This work was completed utilizing the Holland Computing Center of the University of Nebraska, which receives support from the Nebraska Research Initiative.

# Appendix A. Convergence of the PD gradient operator to its classical counterpart

To show the convergence of PD gradient operator  $\mathcal{G}_{\omega}(u)$  to the classical one  $\nabla u$ , we follow a procedure similar to the one used in [70]. Consider an incompressible Newtonian fluid motion in which  $\theta$  is sufficiently smooth in  $\Omega$ , one can write, for any  $\mathbf{x} \in \Omega$  and  $\hat{\mathbf{x}} \in \mathcal{H}_{\mathbf{x}}$  that:

$$\hat{u} - u = \xi_i u_{,i} + \frac{1}{2} \xi_i \xi_j u_{,ij} + \frac{1}{3!} \xi_i \xi_j \xi_k u_{,ijk} + \dots \quad i, j, k \in [1, d]$$
(41)

where  $\boldsymbol{\xi} = (\hat{\boldsymbol{x}} - \boldsymbol{x}) = \boldsymbol{\xi} \boldsymbol{e} = \boldsymbol{\xi}_i \boldsymbol{e}_i$  and d is the space dimension. Substitute Eq. (41), without the remaining terms, into  $\mathcal{G}_{\omega}(u)$  and consider symmetry of  $\mathcal{H}_{\boldsymbol{x}}$ , we get:

$$\mathcal{G}_{\omega}(u) = \int_{\mathcal{H}_{\mathbf{x}}} \omega \left( \hat{u} - u \right) \mathbf{e} d\hat{\mathbf{x}} = \frac{\alpha}{V_{\mathcal{H}}} \int_{\mathcal{H}_{\mathbf{x}}} \frac{1}{\xi} \left\{ \xi_{i} u_{,i} + \frac{1}{3!} \xi_{i} \xi_{j} \xi_{k} u_{,ijk} \right\} \mathbf{e} d\hat{\mathbf{x}} 
= \frac{\alpha}{V_{\mathcal{H}}} \int_{\mathcal{H}_{\mathbf{x}}} \frac{\xi_{i}}{\xi} u_{,i} \mathbf{e} d\hat{\mathbf{x}} + \frac{\alpha}{6V_{\mathcal{H}}} \int_{\mathcal{H}_{\mathbf{x}}} \frac{\xi_{i}}{\xi} \frac{\xi_{j}}{\xi} \frac{\xi_{k}}{\xi} u_{,ijk} \mathbf{e} \xi^{2} d\hat{\mathbf{x}}$$
(42)

If d = 2, we have

$$\mathcal{G}_{\omega}(u) = \frac{\alpha}{V_{\mathcal{H}}} \int_{\mathcal{H}_{\mathbf{x}}} \frac{\xi_{i}}{\xi} u_{,i} \boldsymbol{e} d\hat{\boldsymbol{x}} + \frac{\alpha}{6V_{\mathcal{H}}} \int_{\mathcal{H}_{\mathbf{x}}} \frac{\xi_{i}}{\xi} \frac{\xi_{j}}{\xi} \frac{\xi_{k}}{\xi} u_{,ijk} \boldsymbol{e} \xi^{2} d\hat{\boldsymbol{x}}$$

$$= \frac{\alpha}{\pi \delta^{2}} \int_{0}^{2\pi} \int_{0}^{\delta} \left( \cos \theta \frac{\partial u}{\partial x} (\boldsymbol{x}) + \sin \theta \frac{\partial u}{\partial y} (\boldsymbol{x}) \right) \begin{bmatrix} \cos \theta \\ \sin \theta \end{bmatrix} r dr d\theta$$

$$+ \frac{\alpha}{6\pi \delta^{2}} \int_{0}^{2\pi} \int_{0}^{\delta} \left( \cos^{3} \theta \frac{\partial^{3} u}{\partial x^{3}} (\boldsymbol{x}) + 3 \cos^{2} \theta \sin \theta \frac{\partial^{3} u}{\partial x^{2} \partial y} (\boldsymbol{x}) \right)$$

$$+ 3 \cos \theta \sin^{2} \theta \frac{\partial^{3} u}{\partial x \partial y^{2}} (\boldsymbol{x}) + \sin^{3} \theta \frac{\partial^{3} u}{\partial y^{3}} (\boldsymbol{x}) \right) \begin{bmatrix} \cos \theta \\ \sin \theta \end{bmatrix} r^{3} dr d\theta$$

$$= \frac{\alpha}{\pi \delta^{2}} \frac{\pi \delta^{2}}{2} \nabla \rho (\boldsymbol{x}) + O \left( \delta^{2} \right) = \frac{\alpha}{2} \nabla \rho (\boldsymbol{x}) + O \left( \delta^{2} \right) \tag{43}$$

Similarly, for d = 3, we can show that

$$\mathcal{G}_{\omega}(u) = \frac{\alpha}{3} \nabla \rho \left( \mathbf{x} \right) + O\left(\delta^{2}\right) \tag{44}$$

Therefore, if we set  $\alpha = d$ , the PD operator will converge to the classical one pointwise as  $\delta \to 0$ . For more details, and a proof of convergence in the  $L^2$  norm, the reader is referred to [47].

Note that boundary effects are not considered here. For those PD points near the boundary which do not have a complete horizon region, the above convergence does not stand unless special treatments are provided (e.g., fictitious nodes methods [56,58]).

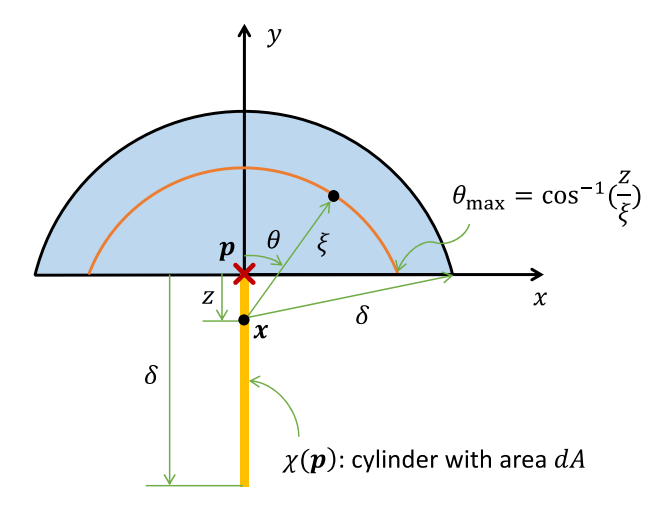


Fig. 10. Computation of force per unit area, at a generic point p, from bond force densities (redrawn from [12]).

### Appendix B. Computing PD stress component from bond force densities

To compute the shear stress at an arbitrary point p in the PD model, we first consider a plane intersecting p and normal to the y-axis and a thin cylinder below p with cross-sectional area dA and length  $\delta$ , where  $\delta$  is the horizon of the PD model. Force through the plane on the cylinder is carried through the bonds that have one end in the cylinder and the other end on the other side of the plane. A typical point x in the cylinder is located a distance z to the bottom of the plane, with  $0 < z \le \delta$  (Fig. 10). The force density (per unit volume square) in a typical bond connecting this point to the other side of the plane is given by  $f(x, \hat{x})$ . Using a spherical coordinate system in which  $\phi$  is the angle from the y-axis, and  $\xi$  is the bond length, the total force on the cylinder is then (in 3D) [12] (Fig. 10):

$$d\mathbf{F} = dA \int_{0}^{2\pi} \int_{0}^{\delta} \int_{0}^{\xi} \int_{0}^{\cos^{-1}\left(\frac{z}{\xi}\right)} \mathbf{f}(\xi, \phi, \theta) \xi^{2} \sin\phi d\phi dz d\xi d\theta$$
(45)

The shear stress component at p is then given by:

$$\tau_{xx}^{PD} = \frac{\mathrm{d}F_x}{\mathrm{d}A} = \int_{0}^{2\pi} \int_{0}^{\delta} \int_{0}^{\xi} \int_{0}^{\cos^{-1}\left(\frac{z}{\xi}\right)} f_x(\xi,\phi,\theta) \xi^2 \sin\phi \mathrm{d}\phi \mathrm{d}z \mathrm{d}\xi \,\mathrm{d}\theta \tag{46}$$

From Section 2.3, we know that:

$$\mathbf{f} = \frac{\mu \alpha_{\mu}}{V_{\mathcal{H}}} \frac{\left( (\mathbf{I} - \mathbf{e} \otimes \mathbf{e}) \left( \hat{\mathbf{v}} - \mathbf{v} \right) \right)}{\|\hat{\mathbf{x}} - \mathbf{x}\|^2}$$
(47)

For the fluid flow parallel to the x-axis and with a magnitude of  $v_0y$ , we have

$$f_{x} = \frac{\mu \alpha_{\mu}}{V_{\mathcal{H}}} \frac{\left(1 - \sin^{2} \theta\right)}{\left\|\hat{\mathbf{x}} - \mathbf{x}\right\|^{2}} v_{0} \left(\hat{y} - y\right) \tag{48}$$

Therefore, we can compute the PD shear stress (flux) from the PD bond density of shear force as follows:

$$\tau_{xx}^{PD} = \frac{\mu \alpha_{\mu}}{V_{\mathcal{H}}} \int_{0}^{2\pi} \int_{0}^{\delta} \int_{0}^{\xi} \int_{0}^{\cos^{-1}\left(\frac{z}{\xi}\right)} \frac{1}{\xi^{2}} \left(1 - \sin^{2}\theta\right) v_{0} \left(\hat{y} - y\right) \xi^{2} \sin\phi d\phi dz d\xi d\theta =$$

$$= -\frac{3\alpha_{\mu}\mu v_{0}}{2\delta^{3}} \int_{0}^{\delta} \int_{0}^{\xi} \int_{0}^{\cos^{-1}\left(\frac{z}{\xi}\right)} \xi \cos^{3}\phi d\cos\phi dz d\xi$$

$$= -\frac{3\alpha_{\mu}\mu\nu_{0}}{8\delta^{3}} \int_{0}^{\delta} \xi \int_{0}^{\xi} \left(\frac{z^{4}}{\xi^{4}} - 1\right) dz d\xi = \frac{3\alpha_{\mu}\mu\nu_{0}}{10\delta^{3}} \int_{0}^{\delta} \xi^{2} d\xi = \frac{\alpha_{\mu}\mu\nu_{0}}{10}$$
(49)

Similarly, for 2D, we have:

$$\begin{split} \tau_{xx}^{\text{PD}} &= \int\limits_{0}^{\delta} \int\limits_{0}^{\xi} \int\limits_{0}^{\cos^{-1}\left(\frac{\xi}{\xi}\right)} \int\limits_{0}^{f} f_{x}\xi \, d\theta \, dz \, d\xi \\ &= \frac{\mu\alpha_{\mu}}{\nu_{\mathcal{H}}} \int\limits_{0}^{\delta} \int\limits_{0}^{\xi} \int\limits_{0}^{\cos^{-1}\left(\frac{\xi}{\xi}\right)} \frac{1}{\xi^{2}} \left(1 - \sin^{2}\theta\right) \nu_{0} \left(\hat{y} - y\right) \xi \, d\theta \, dz \, d\xi = \frac{\alpha_{\mu}\mu\nu_{0}}{\pi\delta^{2}} \int\limits_{0}^{\delta} \int\limits_{0}^{\xi} \int\limits_{0}^{\cos^{-1}\left(\frac{\xi}{\xi}\right)} \cos^{3}\theta \, d\theta \, dz \, d\xi \\ &= \frac{\alpha_{\mu}\mu\nu_{0}}{\pi\delta^{2}} \int\limits_{0}^{\delta} \int\limits_{0}^{\xi} \left(\left(\frac{1}{3}\sin\theta\left(2 + \cos^{2}\theta\right)\right) \mid \cos^{-1}\left(\frac{\xi}{\xi}\right)\right) \, d\theta \, dz \, d\xi \\ &= \frac{2\alpha_{\mu}\mu\nu_{0}}{\pi\delta^{2}} \int\limits_{0}^{\delta} \int\limits_{0}^{\xi} \left(\frac{1}{3}\sqrt{1 - \left(\frac{Z}{\xi}\right)^{2}} \left(2 + \left(\frac{Z}{\xi}\right)^{2}\right)\right) \, dz \, d\xi \\ &= \frac{2\alpha_{\mu}\mu\nu_{0}}{\pi\delta^{2}} \int\limits_{0}^{\delta} \xi \int\limits_{0}^{\xi} \left(\frac{1}{3}\sqrt{1 - x^{2}} \left(2 + x^{2}\right)\right) \, dx \, d\xi \\ &= \frac{2\alpha_{\mu}\mu\nu_{0}}{\pi\delta^{2}} \int\limits_{0}^{\delta} \xi \int\limits_{0}^{\xi} \left(\cos^{2}\alpha\left(3 - \cos^{2}\alpha\right)\right) \, d\alpha \, d\xi \\ &= \frac{2\alpha_{\mu}\mu\nu_{0}}{3\pi\delta^{2}} \int\limits_{0}^{\delta} \xi \int\limits_{0}^{\xi} \left(\cos^{2}\alpha\left(3 - \cos^{2}\alpha\right)\right) \, d\alpha \, d\xi \\ &= \frac{2\alpha_{\mu}\mu\nu_{0}}{3\pi\delta^{2}} \int\limits_{16}^{\delta} \pi \int\limits_{0}^{2} \left(\cos^{2}\alpha\left(3 - \cos^{2}\alpha\right)\right) \, d\alpha \, d\xi \\ &= \frac{2\alpha_{\mu}\mu\nu_{0}}{3\pi\delta^{2}} \int\limits_{16}^{\delta} \pi \int\limits_{0}^{2} \left(\cos^{2}\alpha\left(3 - \cos^{2}\alpha\right)\right) \, d\alpha \, d\xi \end{aligned}$$

# References

- [1] R. Metzler, J. Klafter, The random walk's guide to anomalous diffusion: a fractional dynamics approach, Phys. Rep. 339 (2000) 1–77, https://doi.org/10.1016/S0370-1573(00)00070-3.
- [2] R. Metzler, J. Klafter, The restaurant at the end of the random walk: recent developments in the description of anomalous transport by fractional dynamics, J. Phys. A, Math. Gen. 37 (2004), https://doi.org/10.1088/0305-4470/37/31/R01.
- [3] M. Samiee, A. Akhavan-Safaei, M. Zayernouri, A fractional subgrid-scale model for turbulent flows: theoretical formulation and a priori study, Phys. Fluids 32 (2020) 055102, https://doi.org/10.1063/1.5128379.
- [4] M.F. Shlesinger, B.J. West, J. Klafter, Lévy dynamics of enhanced diffusion: application to turbulence, Phys. Rev. Lett. 58 (1987) 1100–1103, https://doi.org/10.1103/PhysRevLett.58.1100.
- [5] B.A. Carreras, V.E. Lynch, G.M. Zaslavsky, Anomalous diffusion and exit time distribution of particle tracers in plasma turbulence model, Phys. Plasmas 8 (2001) 5096–5103, https://doi.org/10.1063/1.1416180.
- [6] S.A. Silling, Origin and effect of nonlocality in a composite, J. Mech. Mater. Struct. 9 (2014) 245–258, https://doi.org/10.2140/jomms.2014.9.245.
- [7] J. Zhao, Z. Chen, J. Mehrmashhadi, F. Bobaru, A stochastic multiscale peridynamic model for corrosion-induced fracture in reinforced concrete, Eng. Fract. Mech. 229 (2020) 106969, https://doi.org/10.1016/j.engfracmech.2020.106969.
- [8] S. Duo, H. Wang, Y. Zhang, A comparative study on nonlocal diffusion operators related to the fractional Laplacian, Discrete Contin. Dyn. Syst., Ser. B 24 (2019) 231–256, https://doi.org/10.3934/dcdsb.2018110.
- [9] S.A. Silling, Reformulation of elasticity theory for discontinuities and long-range forces, J. Mech. Phys. Solids 48 (2000) 175–209, https://doi.org/10. 1016/S0022-5096(99)00029-0.
- [10] M. D'Elia, M. Gunzburger, The fractional Laplacian operator on bounded domains as a special case of the nonlocal diffusion operator, Comput. Math. Appl. 66 (2013) 1245–1260, https://doi.org/10.1016/j.camwa.2013.07.022.
- [11] E. Madenci, E. Oterkus, Peridynamic Theory and Its Applications, Springer New York, New York, NY, 2014.
- [12] F. Bobaru, J.T. Foster, P.H. Geubelle, S.A. Silling, Handbook of Peridynamic Modeling, CRC Press, 2016.
- [13] H. Ouchi, A. Katiyar, J. York, J.T. Foster, M.M. Sharma, A fully coupled porous flow and geomechanics model for fluid driven cracks: a peridynamics approach, Comput. Mech. 55 (2015) 561–576, https://doi.org/10.1007/s00466-015-1123-8.
- [14] S. Oterkus, E. Madenci, E. Oterkus, Fully coupled poroelastic peridynamic formulation for fluid-filled fractures, Eng. Geol. 225 (2017) 19–28, https://doi.org/10.1016/j.enggeo.2017.02.001.
- [15] E. Askari, F. Bobaru, R.B. Lehoucq, M.L. Parks, S.A. Silling, O. Weckner, Peridynamics for multiscale materials modeling, J. Phys. Conf. Ser. 125 (2008) 012078, https://doi.org/10.1088/1742-6596/125/1/012078.

- [16] A. Javili, R. Morasata, E. Oterkus, S. Oterkus, Peridynamics review, Math. Mech. Solids 24 (2019) 3714-3739, https://doi.org/10.1177/1081286518803411.
- [17] A. Katiyar, J.T. Foster, H. Ouchi, M.M. Sharma, A peridynamic formulation of pressure driven convective fluid transport in porous media, J. Comput. Phys. 261 (2014) 209–229. https://doi.org/10.1016/j.icp.2013.12.039.
- [18] S.A. Silling, Stability of peridynamic correspondence material models and their particle discretizations, Comput. Methods Appl. Mech. Eng. 322 (2017) 42–57, https://doi.org/10.1016/j.cma.2017.03.043.
- [19] Q. Tu, S. Li, An updated Lagrangian particle hydrodynamics (ULPH) for Newtonian fluids, J. Comput. Phys. 348 (2017) 493–513, https://doi.org/10.1016/j.jcp.2017.07.031.
- [20] J. Yan, S. Li, A.M. Zhang, X. Kan, P.N. Sun, Updated Lagrangian Particle Hydrodynamics (ULPH) modeling and simulation of multiphase flows, J. Comput. Phys. 393 (2019) 406–437, https://doi.org/10.1016/j.jcp.2019.05.017.
- [21] J. Yan, S. Li, X. Kan, A.M. Zhang, X. Lai, Higher-order nonlocal theory of Updated Lagrangian Particle Hydrodynamics (ULPH) and simulations of multiphase flows, Comput. Methods Appl. Mech. Eng. 368 (2020) 113176, https://doi.org/10.1016/J.CMA.2020.113176.
- [22] J. Yan, S. Li, X. Kan, A.M. Zhang, L. Liu, Updated Lagrangian particle hydrodynamics (ULPH) modeling of solid object water entry problems, Comput. Mech. 67 (2021) 1685–1703, https://doi.org/10.1007/S00466-021-02014-4/FIGURES/13.
- [23] J. Wang, X. Zhang, Improved moving particle semi-implicit method for multiphase flow with discontinuity, Comput. Methods Appl. Mech. Eng. 346 (2019) 312–331, https://doi.org/10.1016/j.cma.2018.12.009.
- [24] M.A. Bessa, J.T. Foster, T. Belytschko, W.K. Liu, A meshfree unification: reproducing kernel peridynamics, Comput. Mech. 53 (2014) 1251–1264, https://doi.org/10.1007/s00466-013-0969-x.
- [25] G.C. Ganzenmüller, S. Hiermaier, M. May, On the similarity of meshless discretizations of peridynamics and smooth-particle hydrodynamics, Comput. Struct. 150 (2015) 71–78, https://doi.org/10.1016/j.compstruc.2014.12.011.
- [26] Y. Gao, S. Oterkus, Nonlocal numerical simulation of low Reynolds number laminar fluid motion by using peridynamic differential operator, Ocean Eng. 179 (2019) 135–158, https://doi.org/10.1016/j.oceaneng.2019.03.035.
- [27] Y. Gao, S. Oterkus, Multi-phase fluid flow simulation by using peridynamic differential operator, Ocean Eng. 216 (2020) 108081, https://doi.org/10.1016/j.oceaneng.2020.108081.
- [28] Y. Mikata, Peridynamics for fluid mechanics and acoustics, Acta Mech. 232 (2021) 3011-3032, https://doi.org/10.1007/s00707-021-02947-0.
- [29] C.G. Wagner, M.M. Norton, J.S. Park, P. Grover, Exact coherent structures and phase space geometry of preturbulent 2D active nematic channel flow, Phys. Rev. Lett. 128 (2022) 028003, https://doi.org/10.1103/PhysRevLett.128.028003.
- [30] Q. Du, J.R. Kamm, R.B. Lehoucq, M.L. Parks, A new approach for a nonlocal, nonlinear conservation law, SIAM J. Appl. Math. 72 (2012) 464–487, https://doi.org/10.1137/110833233.
- [31] C. Imbert, R. Shvydkoy, F. Vigneron, Global well-posedness of a non-local Burgers equation: the periodic case, Ann. Fac. Sci. Univ. Toulouse Sci. Math. Sci. Phys. 25 (2016) 723–758, https://doi.org/10.5802/afst.1509.
- [32] C. Foias, Private Communication, College Station, TX, 2013.
- [33] F. Bobaru, A. Larios, I. Safarik, C. Victor, J. Zhao, Convergence of solutions to a nonlinear conservation law to solutions of a local conservation law, in preparation, (n.d.).
- [34] J. Mehrmashhadi, Z. Chen, J. Zhao, F. Bobaru, A stochastically homogenized peridynamic model for intraply fracture in fiber-reinforced composites, Compos. Sci. Technol. 182 (2019), https://doi.org/10.1016/j.compscitech.2019.107770.
- [35] Z. Chen, S. Niazi, F. Bobaru, A peridynamic model for brittle damage and fracture in porous materials, Int. J. Rock Mech. Min. Sci. 122 (2019) 104059, https://doi.org/10.1016/j.ijrmms.2019.104059.
- [36] W. Hu, Y. Wang, J. Yu, C.-F. Yen, F. Bobaru, Impact damage on a thin glass plate with a thin polycarbonate backing, Int. J. Impact Eng. 62 (2013) 152–165, https://doi.org/10.1016/j.ijimpeng.2013.07.001.
- [37] G. Zhang, G.A. Gazonas, F. Bobaru, Supershear damage propagation and sub-Rayleigh crack growth from edge-on impact: a peridynamic analysis, Int. J. Impact Eng. 113 (2018) 73–87, https://doi.org/10.1016/j.ijimpeng.2017.11.010.
- [38] F. Mousavi, S. Jafarzadeh, F. Bobaru, An ordinary state-based peridynamic elastoplastic 2D model consistent with J2 plasticity, Int. J. Solids Struct. 229 (2021) 111146. https://doi.org/10.1016/j.ijsolstr.2021.111146.
- [39] F. Bobaru, M. Duangpanya, The peridynamic formulation for transient heat conduction, Int. J. Heat Mass Transf. 53 (2010) 4047–4059, https://doi.org/10.1016/j.ijheatmasstransfer.2010.05.024.
- [40] F. Bobaru, M. Duangpanya, A peridynamic formulation for transient heat conduction in bodies with evolving discontinuities, J. Comput. Phys. 231 (2012) 2764–2785, https://doi.org/10.1016/j.jcp.2011.12.017.
- [41] J. Zhao, Z. Chen, J. Mehrmashhadi, F. Bobaru, Construction of a peridynamic model for transient advection-diffusion problems, Int. J. Heat Mass Transf. 126 (2018) 1253–1266, https://doi.org/10.1016/j.ijheatmasstransfer.2018.06.075.
- [42] Z. Chen, F. Bobaru, Peridynamic modeling of pitting corrosion damage, J. Mech. Phys. Solids 78 (2015) 352–381, https://doi.org/10.1016/j.jmps.2015.02. 015.
- [43] S. Jafarzadeh, Z. Chen, J. Zhao, F. Bobaru, Pitting, lacy covers, and pit merger in stainless steel: 3D peridynamic models, Corros. Sci. 150 (2019) 17–31, https://doi.org/10.1016/j.corsci.2019.01.006.
- [44] J. Zhao, S. Jafarzadeh, M. Rahmani, Z. Chen, Y.-R. Kim, F. Bobaru, A peridynamic model for galvanic corrosion and fracture, Electrochim. Acta 391 (2021) 138968, https://doi.org/10.1016/j.electacta.2021.138968.
- [45] S. Jafarzadeh, J. Zhao, M. Shakouri, F. Bobaru, A peridynamic model for crevice corrosion damage, Electrochim. Acta 401 (2022) 139512, https://doi.org/10.1016/j.electacta.2021.139512.
- [46] A.J. Chorin, J.E. Marsden, A Mathematical Introduction to Fluid Mechanics, Springer New York, New York, NY, 1993.
- [47] Q. Du, M. Gunzburger, R.B. Lehoucq, K. Zhou, A nonlocal vector calculus, nonlocal volume-constrained problems, and nonlocal balance laws, Math. Models Methods Appl. Sci. 23 (2013) 493–540, https://doi.org/10.1142/S0218202512500546.
- [48] N. Prakash, G.D. Seidel, A novel two-parameter linear elastic constitutive model for bond based peridynamics, in: 56th AIAA/ASCE/AHS/ASC Struct. Struct. Dyn. Mater. Conf., American Institute of Aeronautics and Astronautics, Reston, Virginia, 2015.
- [49] Q. Zhu, T. Ni, Peridynamic formulations enriched with bond rotation effects, Int. J. Eng. Sci. 121 (2017) 118–129, https://doi.org/10.1016/j.ijengsci.2017. 09.004.
- [50] A.J. Chorin, A numerical method for solving incompressible viscous flow problems, J. Comput. Phys. 135 (1997) 118–125, https://doi.org/10.1006/jcph. 1997.5716.
- [51] J.J. Monaghan, Simulating free surface flows with SPH, J. Comput. Phys. 110 (1994) 399-406, https://doi.org/10.1006/jcph.1994.1034.
- [52] J.P. Morris, P.J. Fox, Y. Zhu, Modeling low Reynolds number incompressible flows using SPH, J. Comput. Phys. 136 (1997) 214–226, https://doi.org/10. 1006/jcph.1997.5776.
- [53] G.K. Batchelor, An Introduction to Fluid Dynamics, Cambridge University Press, 2000.
- [54] S. Oterkus, E. Madenci, A. Agwai, Peridynamic thermal diffusion, J. Comput. Phys. 265 (2014) 71-96, https://doi.org/10.1016/j.jcp.2014.01.027.
- [55] Y. Tao, X. Tian, Q. Du, Nonlocal diffusion and peridynamic models with Neumann type constraints and their numerical approximations, Appl. Math. Comput. 305 (2017) 282–298, https://doi.org/10.1016/j.amc.2017.01.061.
- [56] Q.V. Le, F. Bobaru, Surface corrections for peridynamic models in elasticity and fracture, Comput. Mech. 61 (2018) 499–518, https://doi.org/10.1007/s00466-017-1469-1.

- [57] J.F. Wendt, J.D. Anderson, J. Degroote, G. Degrez, E. Dick, R. Grundmann, J. Vierendeels, Computational Fluid Dynamics, Springer Berlin Heidelberg, Berlin, Heidelberg, 2009.
- [58] J. Zhao, S. Jafaraadeh, Z. Chen, F. Bobaru, An algorithm for imposing local boundary conditions in peridynamic models on arbitrary domains, EngrXiv (2020), https://doi.org/10.31224/osf.io/7z8qr.
- [59] S.A. Silling, E. Askari, A meshfree method based on the peridynamic model of solid mechanics, Comput. Struct. 83 (2005) 1526–1535, https://doi.org/10.1016/j.compstruc.2004.11.026.
- [60] F. Bobaru, Y.D. Ha, Adaptive refinement and multiscale modeling in 2D peridynamics, Int. J. Multiscale Comput. Eng. 9 (2011) 635–659, https://doi.org/
- [61] S.F. Henke, S. Shanbhag, Mesh sensitivity in peridynamic simulations, Comput. Phys. Commun. 185 (2014) 181–193, https://doi.org/10.1016/j.cpc.2013. 09.010.
- [62] X. Gu, Q. Zhang, X. Xia, Voronoi-based peridynamics and cracking analysis with adaptive refinement, Int. J. Numer. Methods Eng. 112 (2017) 2087–2109, https://doi.org/10.1002/nme.5596.
- [63] S. Li, Z. Chen, L. Tan, F. Bobaru, Corrosion-induced embrittlement in ZK60A Mg alloy, Mater. Sci. Eng. A 713 (2018) 7–17, https://doi.org/10.1016/j.msea. 2017.12.053.
- [64] W. Hu, Y.D. Ha, F. Bobaru, Numerical integration in peridynamics, Technical report, 2010.
- [65] F. Bobaru, G. Zhang, Why do cracks branch? A peridynamic investigation of dynamic brittle fracture, Int. J. Fract. 196 (2015) 59–98, https://doi.org/10. 1007/s10704-015-0056-8.
- [66] P. Seleson, Improved one-point quadrature algorithms for two-dimensional peridynamic models based on analytical calculations, Comput. Methods Appl. Mech. Eng. 282 (2014) 184–217, https://doi.org/10.1016/j.cma.2014.06.016.
- [67] R. Courant, K. Friedrichs, H. Lewy, Über die partiellen Differenzengleichungen der mathematischen Physik, Math. Ann. 100 (1928) 32–74, https://doi.org/10.1007/BF01448839.
- [68] J.J. Monaghan, Smoothed Particle Hydrodynamics, Annu. Rev. Astron. Astrophys. 30 (1992) 543–574, https://doi.org/10.1146/annurev.aa.30.090192. 002551.
- [69] S. Adami, X.Y. Hu, N.A. Adams, A generalized wall boundary condition for smoothed particle hydrodynamics, J. Comput. Phys. 231 (2012) 7057–7075, https://doi.org/10.1016/j.jcp.2012.05.005.
- [70] S. Prudhomme, P. Diehl, On the treatment of boundary conditions for bond-based peridynamic models, Comput. Methods Appl. Mech. Eng. 372 (2020) 113391, https://doi.org/10.1016/j.cma.2020.113391.